Studies of the Interaction of the Viral Suppressor of RNA Silencing Protein p19 with Small RNAs Using Fluorescence Polarization[†]

Jenny Cheng,[‡,§] Selena M. Sagan,[‡,§,||] Zygmunt J. Jakubek,[‡] and John Paul Pezacki*[,‡,||,⊥]

Steacie Institute for Molecular Sciences, National Research Council of Canada, 100 Sussex Drive, Ottawa, Canada K1A 0R6, Department of Chemistry, University of Ottawa, 10 Marie-Curie, Ottawa, Canada K1N 6N5, and Department of Biochemistry, Microbiology and Immunology and Ottawa Institute of Systems Biology, University of Ottawa, Health Sciences Campus, 451 Smyth Road, Ottawa, Canada K1H 8M5

Received March 7, 2008; Revised Manuscript Received May 22, 2008

ABSTRACT: Tombusviruses use a 19 kDa protein (p19) as a suppressor of the RNA silencing pathway during infection. The p19 protein binds to short-interfering RNA (siRNA) as a dimer and shows a high selectivity for short duplex RNAs over other RNA species. Since p19 can bind to synthetic and RNA silencing generated small RNAs with little sequence dependence and with size selectivity, this protein has utility as a tool for studying RNA silencing pathways in eukaryotes. However, the ability of p19 to serve as a tool for studying RNA silencing pathways may be complicated by the presence of other endogenous small RNAs such as micro-RNAs (miRNAs). To understand the importance of endogenous small RNA components with respect to p19's ability to bind to siRNAs, we examined the interactions of p19 with human miR-122, a 23-nucleotide duplex miRNA containing several mismatched base pairs that is highly abundant in the liver. The binding characteristics were compared with those of an siRNA optimized against the human kinase CSK. The binding studies were performed using fluorescence polarization experiments on duplex oligonucleotides containing Cy3 dye labels at the 5′-end of one of the strands of RNA as well as electrophoretic gel mobility shift assays. Both methods indicate that the synthetic siRNA with no mismatches in base pairing bound with >3-fold selectivity over that of miR-122. Our results suggest that p19 can distinguish between siRNAs and miRNA species, although the difference in binding constants is not so large that interactions with endogenous miRNAs can be totally ignored.

The RNA silencing pathway involves the biogenesis of siRNA molecules and is an important antiviral pathway in eukaryotes (*1*–*3*). Tombusviruses use a 19 kDa protein, p19, that acts as an siRNA inhibitor, to evade the RNA silencing host response (*4, 5*). The p19 protein selectively binds to siRNA in a size-selective manner with little dependence on nucleic acid sequence (*6*–*8*). The unique binding properties of p19 have already been exploited for the study of small RNAs in both plant and mammalian systems (*8*–*15*). For example, p19−GFP fusion proteins have been used for localization and temporal studies during viral infections in plants (*15*). The p19 protein has also been used to characterize the small RNAs in mouse embryonic stem cells (*8*). In addition, more stable and higher-affinity variants of p19 have also been engineered (*16*). Thus, a better understanding of the binding properties and selectivity of p19 will aid in its further utility as a tool for probing small RNAs in a number of eukaryotic systems.

Fluorescence polarization measurements have been used extensively to take detailed and accurate measurements of protein−nucleic acid interactions (*17*). This technique relies on a change in rotational diffusion upon binding and the decorrelation of polarization in fluorescence. Fluorescence polarization has been used to study the tetramer−dimer equilibrium of the λ repressor (*18*), aptamer protein interactions (*19*), domain−domain interactions (*20*), and DNA−p53 binding through its C-terminal domain (*21*). Here we demonstrate that this approach is also well suited to assessing protein−RNA interactions of the p19 protein with small RNAs, including both miRNAs[1] and siRNAs.

The small RNA component of a eukaryotic cell can arise transcriptionally (*22*) as well as from the processing of cytoplasmic double-stranded RNA intermediates by the RNA silencing pathway (Figure 1). miRNAs make up a class of endogenously produced noncoding small RNA molecules that are transcriptionally derived. miRNAs are generally ∼21−25 nucleotides (nt) in length, are expressed in a developmental-

[†] This work was supported in part by the Genomics and Health Initiative of the National Research Council. S.M.S. thanks the Natural Sciences and Engineering Research Council for funding in the form of a Graduate Scholarship.

* To whom correspondence should be addressed. E-mail: John.Pezacki@nrc-cnrc.gc.ca. Telephone: (613) 993-7253. Fax: (613) 941-8447.

[‡] National Research Council of Canada.

[§] These authors contributed equally to this work.

[||] Department of Biochemistry, Microbiology and Immunology and Ottawa Institute of Systems Biology, University of Ottawa.

[⊥] Department of Chemistry, University of Ottawa.

[1] Abbreviations: siRNA, short-interfering RNA; miRNA, microRNA; ssRNA, single-stranded RNA; dsRNA, double-stranded RNA; RISC, RNA-induced silencing complex; HCV, hepatitis C virus; EMSA, electrophoretic mobility shift assays; CSK, carboxyl-terminal Src kinase; miR-122, microRNA 122; CIRV, Carnation Italian Ringspot virus; His_8 tag, octahistidine tag; ARM, arginine-rich motif.

10.1021/bi800401y CCC: $40.75
Published on Web 07/03/2008

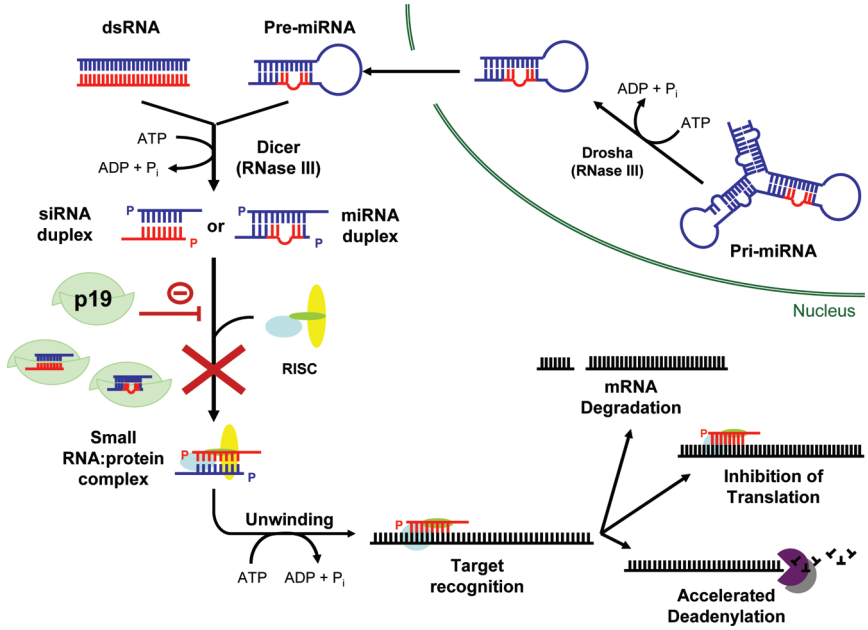

FIGURE 1: Schematic representation of the small RNA suppressor activities of p19 in eukaryotes. Small RNAs can arise transcriptionally from primary miRNAs (pri-miRNAs) or can be derived from dsRNAs in the cytoplasm. Small RNAs (siRNAs and miRNAs) are taken up by the RNA-induced silencing complex (RISC) and unwound, and one strand of the small RNA is used to target complementary mRNAs for degradation, translational inhibition, or accelerated deadenylation. The p19 protein binds to small RNA duplexes and prevents their incorporation into the RISC complex and hence the downstream effects of the small RNAs on gene expression.

and tissue-specific manner, and have been found in all metazoa studied to date (*22, 23*). A number of viral genomes have also been demonstrated to encode miRNAs that can regulate viral and/or host gene expression (*24*). In principle, the p19 protein can interact with small RNAs derived from both sources and influence the regulatory and/or antiviral roles of these small RNAs. In this study, we have chosen to investigate the binding of the p19 protein to two important small RNAs that influence hepatitis C virus (HCV) replication in human hepatocytes, miR-122 and CSK (Figure 2A). miR-122 is a liver-specific miRNA that comprises ~70% of the total miRNAs found in the liver (*25, 26*). The level of miR-122 expression correlates positively with HCV replication, and miR-122 has been demonstrated to interact with the 5′ noncoding region of the HCV RNA genome, facilitating viral replication (*27*). Since miR-122 has been demonstrated to have a positive outcome on HCV replication, sequestration of miR-122 could lead to a novel antiviral strategy. The second small RNA that we chose to study, CSK siRNA, is a synthetic siRNA that downregulates carboxyl-terminal Src kinase (CSK) which influences HCV replication by regulating the phosphorylation of a key viral protein, NS5A (*28*). Herein, we demonstrate that the p19 protein is able to bind to both of these small RNA species, and we have performed detailed binding studies of these interactions using fluorescence polarization and fluorescence-based electrophoretic mobility shift assays (EMSA). The results show that, in principle, p19 may be used to sequester siRNAs and/or miRNAs from diverse sources and has the potential to be used as an antiviral tool to sequester small RNAs that are important for replication or pathogenesis of viruses such as HCV.

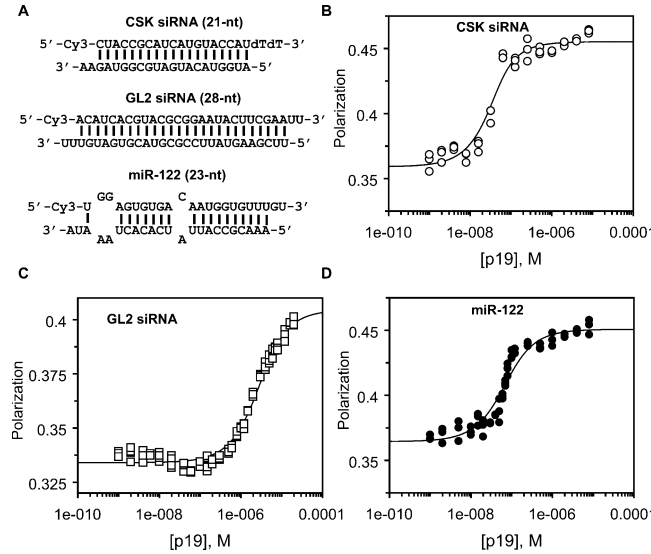

FIGURE 2: Binding curve analyses of CIRV p19 with various small RNAs obtained from fluorescence polarization. (A) Structures of small RNA duplexes. The mispairing of bases in the 23 nt duplex of miR-122 is illustrated showing the bulges in the structure of the miRNA. The binding curves for (B) Cy3-CSK siRNA (21 nt), (C) Cy3-GL2 siRNA (28 nt), and (D) Cy3-miR-122 are shown. The curves were obtained by plotting the change in polarization as a function of the concentration of the p19 dimer using 40 nM small RNA (Cy3-CSK siRNA and Cy3-miR-122) or 2 μM small RNA (Cy3-GL2 siRNA). All measurements were carried out in triplicate.

EXPERIMENTAL PROCEDURES

Expression Plasmid and siRNA Sequences. The histidine-tagged (His-tagged) Carnation Italian Ringspot virus (CIRV) p19 construct (p19) that was used contains a codon-optimized p19 sequence that was subcloned by PCR into the pTriEx 4-neo vector (EMD Biosciences, San Diego, CA) with a C-terminal His_8 tag as described previously (*29*). The siRNAs used were duplex RNA purchased from Dharmacon (Lafayette, CO). siRNA sequences used in this study were as follows: unlabeled CSK 21 nt siRNA, 5′-CUA CCG CAU CAU GUA CCA UdTdT-3′; Cy3-CSK 21 nt siRNA, 5′-Cy3-CUA CCG CAU CAU GUA CCA UdTdT-3′; and Cy3-GL2

28 nt siRNA, 5′-Cy3-ACA UCA CGU ACG CGG AAU ACU UCG AAdT dT-3′. The purity for both CSK and GL2 siRNAs was demonstrated to be >95% according to the manufacturer's specifications. The microRNA duplex (Cy3-miR-122) used in this study was also purchased from Dharmacon with the following sense and antisense sequences, respectively: 5′-UGG AGU GUG ACA AUG GUG UUU GU-3′ and Cy3-5′-AAA CGC CAU UAU CAC ACU AAA UA-3′. miR-122 was deprotected, annealed, and precipitated according to the manufacturer's protocols. To ensure that all of the labeled strands were duplexed, we used a slight excess of the unlabeled strand during annealing of miR-122 duplexes. All RNAs obtained from the manufacturer were PAGE-purified and desalted using reverse-phase HPLC.

Protein Expression and Purification. Bacterial expression of p19 was carried out as previously described (*29*). Briefly, *Escherichia coli* strain BL21(DE3) cells harboring the p19 construct were grown at 37 °C until an OD_{600} of 0.5−0.6 was achieved. Expression of p19 was induced by IPTG at a final concentration of 1 mM. Cultures were then grown for an additional 4−5 h at 30 °C. After the cells had been harvested, bacterial pellets were resuspended in lysis buffer [50 mM NaH_2PO_4, 300 mM NaCl, 10 mM imidazole, 1 mM dithiothreitol (DTT), and 1 mM benzamidine (pH 8.0)] and lysed by sonication on ice. The soluble fraction containing the His-tagged p19 protein was loaded onto a nickel affinity column (GE Healthcare, Piscataway, NJ). After protein binding, the resin was washed with wash buffer [50 mM NaH_2PO_4, 300 mM NaCl, and 60 mM imidazole (pH 8.0)]. Elution of the His-tagged p19 was carried out using elution buffer [50 mM NaH_2PO_4, 300 mM NaCl, and 250 mM imidazole (pH 8.0)], and 10 mM DTT was added immediately to the eluate. The pooled eluates were concentrated to 0.5 mL using the Amicon Ultra 10 kDa MWCO centrifugal filter device (Millipore, Concord, MA). The concentrated samples were then injected into a Superdex 200 size exclusion column (Pharmacia, Peapack, NJ) at a flow rate of 0.5 mL/min. The p19 protein elutes as a stable dimer and is recalcitrant to denaturation even after being boiled for 15−20 min (*13, 16, 29*). Fractions containing the desired p19 proteins, as determined by SDS−PAGE analysis, were pooled and stored at 4 °C for subsequent assays. Pooled p19 fractions were monitored by SDS−PAGE as a single band and estimated to be >95% pure.

Fluorescence Polarization and Data Analysis. Samples were prepared by allowing incubation of 40 nM, 80 nM, 200 nM, or 2 μM Cy3-labeled siRNAs or microRNA with various concentrations of purified p19 in phosphate-buffered saline (PBS) [8 g/L NaCl, 0.2 g/L KCl, 1.44 g/L Na_2HPO_4, and 0.24 g/L KH_2PO_4 (pH 7.4)] with 10 mM DTT at room temperature for 1 h. Fluorescence polarization measurements were then carried out using a Fluorolog Tau-3 Lifetime System (HORIBA Jobin Yvon Inc., Edison, NJ) at room temperature. Polarization was monitored at 560 nm (with a bandwidth of 1 nm) with excitation at 546 nm (with a bandwidth of 6 or 10 nm). Polarization is expressed as

$$P = \frac{I_V - GI_H}{I_V + GI_H} \quad (1)$$

where I_V and I_H are the vertically and horizontally polarized emission intensities, respectively, when vertically polarized light is used to excite the sample. The G factor (measured experimentally) takes into account instrumental effects, and $G = I_{HV}/I_{HH}$, where I_{HV} and I_{HH} are the vertically and horizontally polarized emission intensities, respectively, when horizontally polarized light is used to excite the sample. The polarization of each sample was calculated from an average of 10 measurements each of I_V and I_H, and triplicate values of such a set of averages were collected. The resulting concentration-dependent increase in polarization was plotted against the concentration of the p19 dimer (since the p19 protein binds to one molecule of siRNA as a dimer) (*6, 7*) and fitted according to the following equation:

$$\Delta P = \Delta P_{max}\left[\frac{K_d + np + x}{2np} - \sqrt{\left(\frac{K_d + np + x}{2np}\right)^2 - \frac{x}{np}}\right] \quad (2)$$

where ΔP_{max} denotes the maximal change in polarization, K_d is the dissociation constant, n is the number of equivalent sites on the p19 dimer, p is the concentration of labeled small RNA, and x is the concentration of the p19 dimer.

A competitive study was carried out by premixing 2 μM Cy3-CSK 21 nt siRNA with same molar ratio of the p19 dimer at room temperature for 1 h. Samples were then titrated with increasing concentrations of unlabeled CSK 21 nt siRNA for 1 h at room temperature, and the decrease in fluorescence polarization was measured. The resulting concentration-dependent decrease in polarization was fitted to the following equation:

$$\Delta P = \frac{\Delta P_{max}}{\frac{K_d(K'_d + x)}{K'_d + p} + 1} \quad (3)$$

where ΔP_{max} denotes the maximal change in polarization, K_d is the dissociation constant for one small RNA, K'_d is the dissociation constant for the competing small RNA, p is the concentration of labeled small RNA, and x is the concentration of the unlabeled small RNA.

Electrophoretic Mobility Shift Assays (EMSA) and Data Analysis. For direct binding experiments, samples were prepared by allowing incubation of 40 nM, 80 nM, 200 nM, or 2 μM labeled RNA with various concentrations of purified p19 in buffer containing 20 mM Tris, 100 mM NaCl, 1 mM EDTA, 0.02% (v/v) Triton X-100, and 1 mM tris(2-carboxyethyl)phosphine (TCEP) (pH 7) for 1 h at room temperature. For the competition experiment, 1 μM Cy3-CSK siRNA was premixed with the same molar ratio of the p19 dimer at room temperature for 1 h. Samples were then titrated with various concentrations of unlabeled CSK siRNA for 1 h at room temperature. Two microliters of 5× Hi-Density TBE sample buffer (Novex, Invitrogen Inc.) was added to 18 μL of the binding reaction mixture. Ten microliters of each sample was analyzed by electrophoresis at a constant voltage of 100 V for 1 h through a 6% TBE DNA retardation gel in 1× TBE running buffer (Novex, Invitrogen Inc.). Bands corresponding to bound and free fluorescently labeled siRNAs and miRNAs were quantified with a Molecular Dynamics Typhoon phosphorimager (GE Healthcare) and ImageJ (National Institutes of Health, Bethesda, MD). The data from the direct binding experiments were fitted to eq 2, and the competition binding experiment was fitted to eq 3.

RESULTS

Quantification of p19−Small RNA Interactions in Solution Using Fluorescence Polarization. Fluorescence polarization was used to quantify the binding interactions between the p19 protein and small RNA species (siRNAs and miRNAs). Fluorescence polarization measurements are based on observations of the rotational motion of fluorescently labeled molecules in solution and do not require the separation of bound and free ligand. Thus, information about the true equilibrium of the molecular interactions can be obtained using this technique (*17, 30*). For example, when linearly polarized light is used to excite a rapidly rotating fluorophore-conjugated small RNA molecule in solution, the emitted light will rapidly become depolarized. However, when the fluorophore-conjugated small RNA molecule is bound by p19, the larger complex tumbles much slower in solution and the emitted light will remain polarized on a significantly longer time scale. In our experiments, the small RNAs were conjugated to the Cy3 fluorophore. Initially, the optimal wavelengths for excitation (546 nm) and emission (560 nm) were determined according to the excitation and emission spectra of Cy3. To determine the minimum concentration of the fluorophore that gives a detectable intensity by the instrument, samples with various concentrations of the Cy3 dye were excited at 546 nm and the vertical and horizontal components of the emitted light were measured at 560 nm. It was found that fluorescence could be measured with a sufficient signal-to-noise ratio at concentrations as low as 40 nM. We performed similar experiments on the Cy3-conjugated small RNA samples. The measurements taken with the Cy3-conjugated small RNAs verified that the conjugation of the Cy3 fluorophore to the small RNA did not result in a change in the excitation and emission spectra of Cy3. In addition, varying the concentration of the Cy3-conjugated small RNA did not have a significant effect on polarization. However, as expected, the polarization of the Cy3-conjugated small RNA was significantly greater than that of the Cy3 fluorophore alone due to the overall increase in molecular weight.

Next we investigated the dependence of fluorescence polarization of Cy3-conjugated CSK siRNA in the presence of p19. All fluorescence polarization measurements were carried out in buffer containing PBS (pH 7.4), designed to mimic physiological conditions, and 10 mM DTT, used to prevent aggregation of p19 due to nonspecific disulfide linkage of cysteine residues. The total fluorescence intensity was monitored and remained constant throughout the duration of each experiment. With the increase in the concentration of p19 in the samples containing a constant concentration of Cy3-CSK siRNA (Figure 2A), there was a gradual increase in polarization implying that binding had occurred between the p19 protein and the siRNA. By plotting the change in polarization as a function of the concentration of p19, we obtained a sigmoidal curve (Figure 2B) signifying a dose−response relationship between the p19 protein and the siRNA. Analysis of the curve indicates a dissociation constant for the p19−Cy3-CSK siRNA interaction of 15 ± 7 nM. The presence of the Cy3 fluorophore on the 5′ end of the siRNA may impede its ability to bind p19 due to steric hindrance. The dissociation constant determined by fluorescence polarization in this study is smaller than the value determined from our previous studies using a fluorescence detection method on Ni^{2+}-NTA-coated plates (*16, 29*) (Table 1). The lower affinity obtained from the fluorescence detection method on Ni^{2+}-NTA-coated plates may be due to the conformational restriction of p19 as a result of surface binding which may hinder its ability to bind to siRNA.

Table 1: Dissociation Constants for CIRV p19 and Small RNAs

	K_d (nM)		
	Ni-NTA[a]	fluorescence polarization	EMSA[b]
Cy3-miR-122 (23 nt)	450 ± 91	15 ± 7	21 ± 3
Cy3-GL2 siRNA (28 nt)	∼35000[c]	1790 ± 182	∼20000[c]
Cy3-CSK siRNA (21 nt)	N/A	47 ± 7	223 ± 43[d] 199 ± 186[e]
unlabeled CSK siRNA	N/A	12 ± 2	7 ± 3

[a] Fluorescence detection with a 96-well Ni-NTA-coated plate. [b] Electrophoretic mobility shift assay performed at 40 nM RNA. [c] Binding experiments were performed at 200 nM siRNA and were not able to reach saturation. [d] Performed with 5′-sense-labeled miR-122. [e] Performed with 5′-antisense-labeled miR-122. Similar values were determined at 200 nM miR-122.

To be certain that the observed change in polarization is due to the binding of functional p19 with the target Cy3-CSK siRNA, we investigated the dependence of the change in fluorescence polarization in the presence of a longer duplex siRNA. The curve obtained from the fluorescence polarization experiment with the 28 nt Cy3-GL2 siRNA (Figure 2A) is shown in Figure 2C. The dissociation constant was estimated to be approximately 1790 ± 182 nM (Table 1), an almost 120-fold decrease in affinity compared to that of the 21 nt Cy3-CSK siRNA. This is consistent with previous results obtained by our group (*29*) and others (*6*) in which p19 was demonstrated to bind with decreasing affinities to siRNAs of increasing length from 21 to 28 nt. We were unable to reach saturation using this siRNA due to the solubility limitations of concentrations of p19 $>20\ \mu$M. This demonstrates the size-selective binding of p19 to siRNA using the fluorescence polarization method which is consistent with the known binding behavior of p19 from previous studies (*6, 16, 29*).

p19 Is Able To Bind to a Human miRNA, miR-122, with Nanomolar Affinity. The binding of p19 with miR-122 was also investigated by fluorescence polarization. miR-122 is a 23 nt miRNA containing several mismatched base pairs resulting in structural irregularities or bulges in the dsRNA duplex when compared to the perfectly complementary siRNA duplex (Figure 2A). Plotting the data from the polarization measurements of Cy3-miR-122 with varying concentrations of p19 also resulted in a sigmoidal curve (Figure 2D) with a dissociation constant of 47 ± 7 nM (Table 1). The binding affinity of p19 for Cy3-miR-122 shows a >3-fold decrease in affinity when compared with that for Cy3-CSK siRNA. The lower affinity is most likely due to the steric hindrance of the bulges arising from mismatched base pairs in the miRNA duplex on p19. However, the affinity did not decrease to the same degree as that of the 28 nt Cy3-GL2 siRNA, perhaps due to the less dramatic length difference of the 23 nt Cy3-miR-122 as compared with the 21 nt Cy3-CSK siRNA. The mismatches in the miR-122 structure may also compress the actual length of the 23 nt miRNA duplex so that it appears slightly shorter, similar to a 21 nt siRNA molecule. As a result, the p19 dimer may be

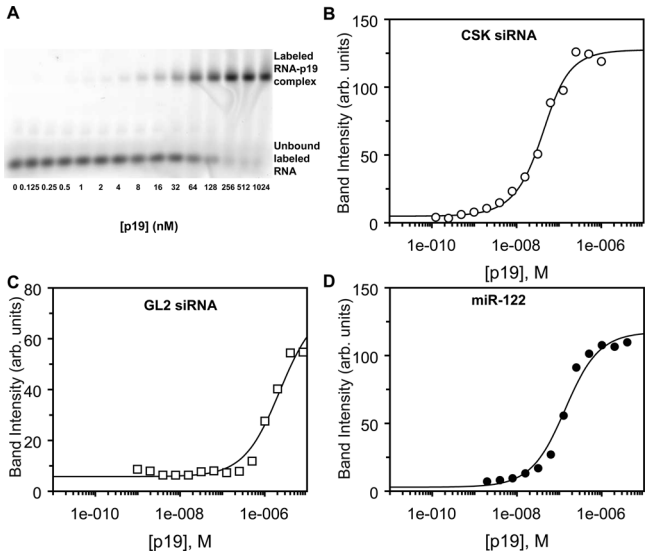

FIGURE 3: Electrophoretic mobility shift assays of p19−small RNA interactions. (A) A representative gel for determining the dissociation constant for p19 and CSK siRNA performed with 40 nM Cy3-CSK siRNA (21 nt) with varying concentrations (0−512 nM) of the p19 dimer. Curves in panels B and C were obtained by plotting the normalized fluorescent band intensities as a function of the concentration of the p19 dimer for the labeled small RNAs (40 nM Cy3-CSK siRNA and Cy3-miR-122; 200 nM GL2 siRNA). The binding curves for (B) Cy3-CSK siRNA (21 nt), (C) Cy3-GL2 siRNA (28 nt), and (D) Cy3-miR-122 (23 nt) are shown.

able to accommodate the miR-122 duplex between the two end-capping helices (see Discussion).

Fluorescence-Based EMSA as an Alternative Method for Assessing p19−Small RNA Interactions. The binding behaviors of p19 with the Cy3-labeled small RNAs examined by fluorescence polarization were also investigated with EMSA. This technique is also commonly used to assess protein−nucleic acid interactions (*31*). In a previous study, conducted by Vargason and colleagues, EMSA were used to analyze the binding affinity and specificity of CIRV p19 with ^{32}P-radiolabeled siRNAs (*6*). For comparison with our fluorescence-based techniques, we performed similar EMSA experiments with fluorophore-labeled small RNAs. In addition, the use of fluorescence labeling as the detection marker for EMSA in place of ^{32}P radiolabeling can avoid the use of radioactivity while retaining similar sensitivities with the use of modern laser-based scanners.

The EMSA experiments were performed by allowing binding of the Cy3-labeled small RNA samples with various concentrations of p19 in solution under conditions similar to those of the fluorescence polarization experiments described above before gel electrophoresis. Figure 3A illustrates a representative EMSA experiment showing the interaction between p19 and the Cy3-CSK siRNA. There is a gradual increase in the fluorescence intensity of the slower migrating bands with an increase in p19 concentration, corresponding to the labeled small RNA population in complex with p19. In contrast, there was a gradual decrease in intensity of the faster migrating bands corresponding to unbound labeled siRNA, indicating an increase in the size of the population of labeled siRNA molecules in complex with p19. The band intensities corresponding to the p19−small RNA complex were measured and plotted as a function of p19 concentration. Curves corresponding to Cy3-CSK siRNA (21 nt) (Figure 3B), Cy3-GL2 siRNA (28 nt) (Figure 3C), and Cy3-miR-122 (Figure 3D) also show a dose−response relationship between the small RNAs and p19. The dissociation constant of p19 in complex with Cy3-CSK siRNA (21 nt) obtained from EMSA (21 ± 3 nM) was comparable to that from fluorescence polarization [15 ± 7 nM (Table 1)]. The EMSA binding curve for Cy3-miR-122 (23 nt) was larger than that obtained by fluorescence polarization [223 ± 43 nM and/or 199 ± 186 nM (Table 1)]. For Cy3-GL2 siRNA (28 nt), the EMSA binding curve did not reach saturation; however, the estimated dissociation constant values are consistent with those obtained by fluorescence polarization (Table 1). This indicates that the binding affinities of p19 in complex with small RNAs obtained by fluorescence polarization and EMSA measurements are consistent with one another.

The 5′-Cy3 Fluorophore Has a Minimal Effect on p19−Small RNA Interactions. To determine whether the presence of the Cy3 fluorophore on the small RNAs used in our study has any effect on p19 binding, we conducted competition experiments with the Cy3-labeled CSK siRNA and unlabeled CSK siRNA for p19 binding using both the fluorescence polarization and EMSA methods. The competition experiments were carried out by allowing incubation of a 1:1 molar ratio of p19 with Cy3-CSK siRNA and then titrating with increasing concentrations of unlabeled CSK siRNA. Fluorescence polarization was measured at each concentration of unlabeled small RNA. Likewise, we conducted the competition experiment by EMSA under similar conditions except that the samples were loaded onto a gel and examined by in-gel fluorescence. We observed that as the unlabeled siRNA concentration was increased, there was a gradual decrease in the fluorescence intensity of the bands corresponding to the labeled small RNA population in complex with p19 as seen in Figure 4A. In contrast, there was a gradual increase in the intensity of the bands corresponding to unbound labeled siRNA, demonstrating the competition between labeled and unlabeled CSK siRNA for binding with p19.

Measurements from back-titration experiments for both fluorescence polarization and EMSA methods were plotted as a function of unlabeled CSK siRNA concentration (Figure 4B,C). The dissociation constants of p19 with unlabeled CSK siRNA were calculated according to eq 3 for the fluorescence polarization (12 ± 2 nM) and EMSA (7 ± 3 nM) experiments, as summarized in Table 1. Surprisingly, the values of the Cy3-labeled and unlabeled CSK siRNAs were similar in magnitude, indicating that the presence of the Cy3 fluorophore has a minimal effect on the binding of p19 to the siRNA. These results also confirm that the lower affinity obtained with the fluorescence detection method on the Ni^{2+}-NTA-coated plate (*16, 29*) was not due to the presence of the Cy3 fluorophore but was likely a result of surface effects. However, the latter fluorescence detection method using 96-well Ni^{2+}-NTA-coated plates is a rapid, high-throughput fluorescence detection method for screening small RNA−p19 interactions.

DISCUSSION

The ability of p19 to bind to various classes of small RNAs, from perfectly complementary siRNAs to more irregularly structured miRNAs, makes it an important tool

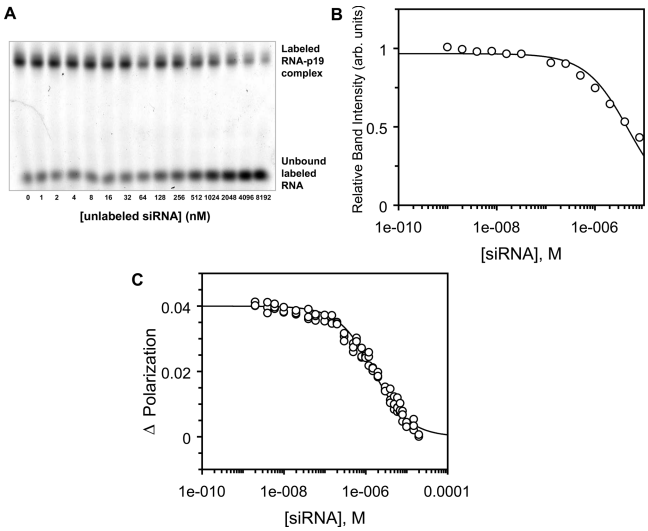

FIGURE 4: Competition experiments with labeled and unlabeled small RNAs. (A) Gel from an EMSA performed with a 1:1 molar ratio of the p19 dimer to Cy3-CSK siRNA (21 nt) with varying concentrations (1−8000 nM) of competitor unlabeled CSK siRNA (21 nt). (B) Competition binding curve obtained by plotting the normalized fluorescent band intensities from panel A as a function of the concentration of competitor unlabeled CSK siRNA. (C) Competition experiment between labeled and unlabeled CSK siRNA with p19 as measured by fluorescence polarization. The competition binding curve was obtained by plotting the change in polarization as a function of the concentration of competitor (unlabeled CSK siRNA). All measurements were carried out in triplicate.

for studying these broad classes of small RNAs in a variety of in vitro and in vivo systems. It has previously been demonstrated that p19 has the ability to bind miRNAs in human cells (*14*), as well as the ability to bind siRNAs of differing lengths (*6, 29*). Since the large class of miRNAs identified to date has a wide degree of secondary structures (*32*), we expect that the degree of complementarity and the varying lengths of the miRNAs will result in a wide degree of p19 binding affinities. In this study, we further characterize the interactions of p19 with a specific irregularly structured miRNA, miR-122, by fluorescence polarization and fluorescence-based EMSA. We demonstrate that p19 can bind miR-122 with nanomolar affinity. The >3-fold reduction in affinity in comparison with p19's interaction with a conventional 21 nt duplex siRNA (CSK siRNA) is likely due to perturbations to the known p19−siRNA interactions as a result of the structural irregularities arising from the base pair mismatches in the miR-122 duplex.

Assuming the 23 nt miR-122 duplex in complex with CIRV p19 adopts a slightly compressed conformation similar in length to that of a perfectly complementary A-form 21 nt siRNA duplex (as in ref *6*), it is likely that the miRNA docks into the protein in a fashion similar to that of the CSK siRNA duplex (Figure 5). If this is the case, the presence of the asymmetric bulges in the miR-122 duplex results in two possible orientations of the miR-122 duplex within the CIRV p19 dimer (Figure 5B,C). Since the interactions of the siRNA molecule with the p19 dimer involve interactions with amino acid residues from both monomer subunits, we will differentiate residues of one p19 monomer from the other by designating them A and B.

In the first orientation (Figure 5B), the bigger (2 nt) bulge will likely affect the interactions of Lys60(A) and Arg18(A) with the miR-122 phosphate backbone. The compression in the length of the miRNA molecule due to the bulges may result in a significant shift in the phosphate backbone which could also have an effect on the interaction with Gln107(A). The smaller (1 nt) bulge is likely to overlap with the position of the central nucleotide (nucleotide 10 from the 5′ end of the sense strand) of CSK siRNA (Figure 5A), as observed in the crystal structure of the CIRV p19-bound siRNA complex (*6*). In this position, the smaller (1 nt) bulge is likely to disrupt the interaction of Ser120(B) and Ser113(B) with the sugar groups of miR-122. Interactions of the Lys67(A), Arg11(A), Arg115(B), and Ser62(B) residues with the miR-122 phosphate backbone are also likely to be at least partially disrupted.

In the second orientation of miR-122 docking into p19 (Figure 5C), the bigger (2 nt) bulge will likely affect the interaction of the Lys60(B) and Arg18(B) residues with the miR-122 phosphate backbone. Since the position of the bigger (2 nt) bulge is opposite to that of the first orientation, a shift in the miR-122 backbone is likely to affect the interaction of the miR-122 sugar and phosphate groups with Gln107(B). In addition, like the first orientation (Figure 5B), the overlap between the smaller (1 nt) bulge with the position of the central nucleotide (nucleotide 10 from the 5′ end of the sense strand) of the CSK siRNA (Figure 5A) is also likely to be slightly shifted. In this case, interactions between the Ser120(B) and Ser113(B) residues and the miR-122 sugar groups and the interaction of the Lys67(A), Arg11(A), and Ser62(B) residues with the phosphate backbone will likely be affected, but the interaction with Arg115(B) is likely to be partially recovered (Figure 5C). The predicted perturbations to the interaction of the p19 residues, known to interact with siRNAs (*6*), with the asymmetric and irregular miR-122 molecule described here, are likely to account for the >3-fold decrease in affinity of p19 for the miR-122 molecule that we observe in the fluorescence polarization measurements (Figure 2 and Table 1).

The capacity of p19 to bind to miR-122 with nanomolar affinity requires the retention of key interactions between p19 and the miR-122 molecule. Electrostatic interactions between the miR-122 phosphate groups and p19 residues Gln107(B), Lys60(A), Arg18(A), Thr40(A), and Trp42(A) and interactions between the sugar groups and Gln107(B), Thr40(A), Thr40(B), and Arg43(A) in the first orientation are far from the bulges, and these contacts are hypothesized to be sustained (Figure 5B). Similarly, interactions between the phosphate groups and Lys60(B), Arg18(B), Thr40(A), Thr40(B), Gln107(A), and Arg115(B) and interactions between the sugar groups and Arg43(A) and Thr40(A) in the second orientation are also likely to remain intact (Figure 5C). Moreover, we anticipate that the end-capping interactions with Trp39 and Trp43 are also maintained and probably account for the bulk of the binding affinity of p19 for miR-122 (Figure 5B,C). As seen in Figure 5A, both ends of the 19 bp duplex region of the 21 nt siRNA are capped by key contacts between the Trp39 and Trp42 residues on each monomer of the p19 dimer. In addition, as demonstrated by Vargason and colleagues, there is a 22-fold decrease in the affinity of p19 for a 23 nt siRNA in comparison with that for a conventional 21 nt siRNA (*6*). However, greater differences in length result in magnitude order decreases in affinity (*6*). Since miR-122 is 23 nt in length, and the bulges are expected to slightly compress the length of the molecule,

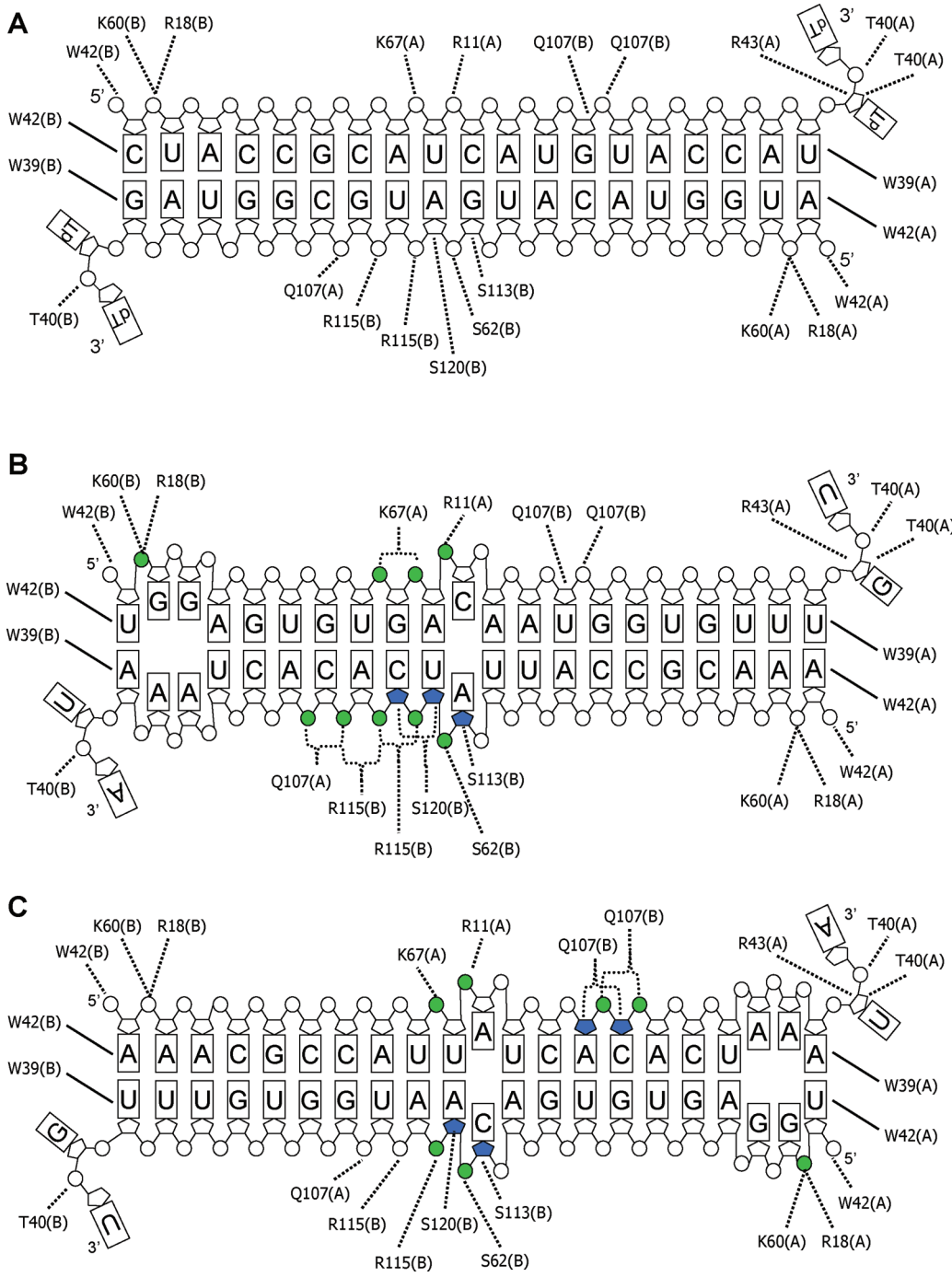

FIGURE 5: Schematic representation of p19 protein−small RNA contacts. (A) Interaction of p19 with CSK siRNA based on the crystal structure of the CIRV p19−siRNA complex described in ref *6*. The proposed interactions between CIRV p19 and miR-122 in orientation 1 and orientation 2 are shown in panels B and C, respectively. The p19 amino acid residues from each monomer subunit are distinguished by designating them A and B. Contacts between amino acid residues and the small RNA phosphate backbone and sugar groups are shown as dashed lines, and stacking interactions are shown as solid lines. Phosphate groups colored green and sugar residues colored blue are the contacts predicted to be disrupted due to the irregular bulges in the miR-122 duplex.

this could allow the duplex region to adopt a length closer to that of the standard 19 bp A-form dsRNA duplex (*33*) to fit between the two end-capping helices of the p19 dimer. Therefore, we anticipate that the p19 end-capping interactions with miR-122 are similar to those with conventional 21 nt siRNA and largely account for the p19−miR-122 binding affinity.

Protein−nucleic acid interactions often involve conformational changes to both the apoprotein and nucleic acid ligand upon binding (*34–37*). These conformational changes facilitate binding by maximizing the number of interactions at the protein−nucleic acid interface. Many nucleic acid-binding proteins alter the shape of their targets upon binding, demonstrating a close relationship between the conformational changes of the nucleic acid to complex formation and binding specificity (*6, 7, 38–41*). For example, in the crystal structure of the *Drosophila* sex-lethal (*Sxl*) protein−RNA complex, the RNA target is sharply bent into a V-shaped conformation within the protein's binding cleft (*41*). More specifically, in the crystal structures of p19−siRNA complexes, there is a 40° bend in the siRNA molecule when bound by p19 (*6, 7*). This bending seems to maximize the

contacts between the siRNA backbone sugar and phosphate groups and the concave binding surface of the p19 dimer. The conformation of the miR-122 molecule may also be adjusted in a similar fashion to maximize its interaction with p19.

Ligand-induced conformational changes in protein structure are also widely recognized in protein−nucleic acid interactions (*42–46*). For example, conformational flexibility is thought to be important for binding of Ro protein to its RNA target (*46*). In addition, in the model of the Dicer enzyme−dsRNA complex, the flexible hinges of the protein are suggested to be crucial for dsRNA binding and processing (*45*). The inherent flexibility of the p19 protein dimer therefore should allow it to tolerate the irregular structure of the miR-122 molecule.

In addition, RNA binding proteins often contain arginine-rich motifs (ARMs) that are able to cross-recognize diverse RNA ligands (*47*). This results from different combinations of electrostatic interactions between multiple Arg residues and the RNA phosphate backbone (*47*). For the p19 protein, the presence of multiple Arg residues in the RNA binding surface (*6, 16, 48*), combined with the inherent flexibility of the protein and nucleic acid ligands, may allow p19 to form new contacts with the miR-122 molecule. These new contacts may compensate for the loss of interactions arising from the bulges in the miR-122 molecule.

CONCLUSION

In conclusion, we have demonstrated that fluorescence polarization and fluorescence-based EMSA experiments can be applied to the study of p19−small RNA interactions. The detailed binding studies of p19 with miR-122 indicate that p19 binds the miRNA with nanomolar affinity. The binding interactions can be understood by the orientations of the miR-122 bulges relative to the key amino acid residues in p19 that interact with siRNA. The ability of p19 to bind to miR-122 and to other miRNAs (*14*) gives it the potential to be used as a versatile tool for the investigation of small RNA function in eukaryotes. Since a number of viruses have been demonstrated to encode their own viral miRNAs or interact with cellular miRNAs (*27, 49, 50*), sequestration and silencing of specific miRNAs in vivo could be a novel approach to inhibiting viral replication. The use of p19 in this way would effectively turn a viral protein into an antiviral agent. However, it is likely that this would necessitate site-directed engineering of the p19 protein for introduction of greater specificity and higher affinity for specific miRNAs, such as miR-122. In addition, the suppression of miRNAs by p19 may serve as a unique approach to understanding the roles of miRNAs in development and disease.

ACKNOWLEDGMENT

We acknowledge the Wildlife Toxicology Division of the National Wildlife Research Center at Carleton University (Ottawa, ON) for the use of the phosphorimager.

REFERENCES

1. Burgyan, J. (2006) Virus induced RNA silencing and suppression: Defence and counter defence. *J. Plant Pathol. 88*, 233–244.
2. Hannon, G. J. (2002) RNA interference. *Nature 418*, 244–251.
3. Baulcombe, D. (2004) RNA silencing in plants. *Nature 431*, 356–363.
4. Russo, M., Burgyan, J., and Martelli, G. P. (1994) Molecular-Biology of Tombusviridae. *Adv. Virus Res. 44*, 381–428.
5. White, K. A., and Nagy, P. D. (2004) Advances in the molecular biology of tombusviruses: Gene expression, genome replication, and recombination. *Prog. Nucleic Acid Res. Mol. Biol. 78*, 187–226.
6. Vargason, J. M., Szittya, G., Burgyan, J., and Hall, T. M. T. (2003) Size selective recognition of siRNA by an RNA silencing suppressor. *Cell 115*, 799–811.
7. Ye, K. Q., Malinina, L., and Patel, D. J. (2003) Recognition of small interfering RNA by a viral suppressor of RNA silencing. *Nature 426*, 874–878.
8. Calabrese, J. M., and Sharp, P. A. (2006) Characterization of the short RNAs bound by the P19 suppressor of RNA silencing in mouse embryonic stem cells. *RNA 12*, 2092–2102.
9. Dunoyer, P., Lecellier, C. H., Parizotto, E. A., Himber, C., and Voinnet, O. (2004) Probing the microRNA and small interfering RNA pathways with virus-encoded suppressors of RNA silencing. *Plant Cell 16*, 1235–1250.
10. Havelda, Z., Hornyik, C., Crescenzi, A., and Burgyan, J. (2003) In situ characterization of *Cymbidium* Ringspot tombusvirus infection-induced posttranscriptional gene silencing in *Nicotiana benthamiana*. *J. Virol. 77*, 6082–6086.
11. Havelda, Z., Hornyik, C., Valoczi, A., and Burgyan, J. (2005) Defective interfering RNA hinders the activity of a tombusvirus-encoded posttranscriptional gene silencing suppressor. *J. Virol. 79*, 450–457.
12. Voinnet, O., Rivas, S., Mestre, P., and Baulcombe, D. (2003) An enhanced transient expression system in plants based on suppression of gene silencing by the p19 protein of tomato bushy stunt virus. *Plant J. 33*, 949–956.
13. Omarov, R., Sparks, K., Smith, L., Zindovic, J., and Scholthof, H. B. (2006) Biological relevance of a stable biochemical interaction between the tombusvirus-encoded P19 and short interfering RNAs. *J. Virol. 80*, 3000–3008.
14. Lecellier, C. H., Dunoyer, P., Arar, K., Lehmann-Che, J., Eyquem, S., Himber, C., Saib, A., and Voinnet, O. (2005) A cellular MicroRNA mediates antiviral defense in human cells. *Science 308*, 557–560.
15. Lakatos, L., Csorba, T., Pantaleo, V., Chapman, E. J., Carrington, J. C., Liu, Y. P., Dolja, V. V., Calvino, L. F., Lopez-Moya, J. J., and Burgyan, J. (2006) Small RNA binding is a common strategy to suppress RNA silencing by several viral suppressors. *EMBO J. 25*, 2768–2780.
16. Cheng, J., Sagan, S. M., Assem, N., Koukiekolo, R., Goto, N. K., and Pezacki, J. P. (2007) Stabilized recombinant suppressors of RNA silencing: Functional effects of linking monomers of Carnation Italian Ringspot virus p19. *Biochim. Biophys. Acta 1774*, 1528–1535.
17. Lundblad, J. R., Laurance, M., and Goodman, R. H. (1996) Fluorescence polarization analysis of protein-DNA and protein-protein interactions. *Mol. Endocrinol. 10*, 607–612.
18. Banik, U., Mandal, N. C., Bhattacharyya, B., and Roy, S. (1993) A Fluorescence Anisotropy Study of Tetramer-Dimer Equilibrium of Lambda-Repressor and Its Implication For Function. *J. Biol. Chem. 268*, 3938–3943.
19. Rusinova, E., Ross, J. B. A., Laue, T. M., Sowers, L. C., and Senear, D. F. (1997) Linkage between operator binding and dimer to octamer self-assembly of bacteriophage lambda cI repressor. *Biochemistry 36*, 12994–13003.
20. Huang, Y. T., Rusinova, E., Ross, J. B. A., and Senear, D. F. (1997) An aromatic stacking interaction between subunits helps mediate DNA sequence specificity: Operator site discrimination by phage lambda cl repressor. *J. Mol. Biol. 267*, 403–417.
21. Weinberg, R. L., Freund, S. M. V., Veprintsev, D. B., Bycroft, M., and Fersht, A. R. (2004) Regulation of DNA binding of p53 by its C-terminal domain. *J. Mol. Biol. 342*, 801–811.
22. Zamore, P. D., and Haley, B. (2005) Ribo-gnome: The big world of small RNAs. *Science 309*, 1519–1524.
23. Ambros, V. (2004) The functions of animal microRNAs. *Nature 431*, 350–355.
24. Sarnow, P., Jopling, C. L., Norman, K. L., Schutz, S., and Wehner, K. A. (2006) MicroRNAs: Expression, avoidance and subversion by vertebrate viruses. *Nat. Rev. Microbiol. 4*, 651–659.
25. Lagos-Quintana, M., Rauhut, R., Yalcin, A., Meyer, J., Lendeckel, W., and Tuschl, T. (2002) Identification of tissue-specific microRNAs from mouse. *Curr. Biol. 12*, 735–739.

26. Chang, J., Nicolas, E., Marks, D., Sander, C., Lerro, A., Buendia, M. A., Xu, C., Mason, W. S., Moloshok, T., Bort, R., Zaret, K. S., and Taylor, J. M. (2004) miR-122, a Mammalian Liver-Specific microRNA, is Processed from hcr mRNA and May Downregulate the High Affinity Cationic Amino Acid Transporter CAT-1. *RNA Biol. 1*, 106–113.
27. Jopling, C. L., Yi, M. K., Lancaster, A. M., Lemon, S. M., and Sarnow, P. (2005) Modulation of hepatitis C virus RNA abundance by a liver-specific microRNA. *Science 309*, 1577–1581.
28. Supekova, L., Supek, F., Lee, J., Chen, S., Gray, N., Pezacki, J. P., Schlapbach, A., and Schultz, P. G. (2008) Identification of human kinases involved in hepatitis C virus replication by small interference RNA library screening. *J. Biol. Chem. 283*, 29–36.
29. Sagan, S. M., Koukiekolo, R., Rodgers, E., Goto, N. K., and Pezacki, J. P. (2007) Inhibition of siRNA binding to a p19 viral suppressor of RNA silencing by cysteine alkylation. *Angew. Chem., Int. Ed. 46*, 2005–2009.
30. Checovich, W. J., Bolger, R. E., and Burke, T. (1995) Fluorescence Polarization: A New Tool For Cell and Molecular Biology. *Nature 375*, 254–256.
31. Lane, D., Prentki, P., and Chandler, M. (1992) Use of Gel Retardation to Analyze Protein-Nucleic Acid Interactions. *Microbiol. Rev. 56*, 509–528.
32. Griffiths-Jones, S., Saini, H. K., van Dongen, S., and Enright, A. J. (2008) miRBase: Tools for microRNA genomics. *Nucleic Acids Res. 36*, D154–D158.
33. Ye, K. Q., and Patel, D. J. (2005) RNA silencing suppressor p21 of beet yellows virus forms an RNA binding octameric ring structure. *Structure 13*, 1375–1384.
34. Steitz, T. A. (1990) Structural Studies of Protein Nucleic-Acid Interaction: The Sources of Sequence-Specific Binding. *Q. Rev. Biophys. 23*, 205–280.
35. Tjian, R., and Maniatis, T. (1994) Transcriptional Activation: A Complex Puzzle With Few Easy Pieces. *Cell 77*, 5–8.
36. Williamson, J. R. (2000) Induced fit in RNA-protein recognition. *Nat. Struct. Biol. 7*, 834–837.
37. Leulliot, N., and Varani, G. (2001) Current topics in RNA-protein recognition: Control of specificity and biological function through induced fit and conformational capture. *Biochemistry 40*, 7947–7956.
38. Werner, M. H., Gronenborn, A. M., and Clore, G. M. (1996) Intercalation, DNA kinking, and the control of transcription. *Science 271*, 778–784.
39. Hard, T., and Lundback, T. (1996) Thermodynamics of sequence-specific protein-DNA interactions. *Biophys. Chem. 62*, 121–139.
40. Dworkin, J., Ninfa, A. J., and Model, P. (1998) A protein-induced DNA bend increases the specificity of a prokaryotic enhancer-binding protein. *Genes Dev. 12*, 894–900.
41. Handa, N., Nureki, O., Kurimoto, K., Kim, I., Sakamoto, H., Shimura, Y., Muto, Y., and Yokoyama, S. (1999) Structural basis for recognition of the tra mRNA precursor by the sex-lethal protein. *Nature 398*, 579–585.
42. Najmanovich, R., Kuttner, J., Sobolev, V., and Edelman, M. (2000) Side-chain flexibility in proteins upon ligand binding. *Proteins: Struct., Funct., Genet. 39*, 261–268.
43. Ma, B., Shatsky, M., Wolfson, H. J., and Nussinov, R. (2002) Multiple diverse ligands binding at a single protein site: A matter of pre-existing populations. *Protein Sci. 11*, 184–197.
44. Gutteridge, A., and Thornton, J. (2005) Conformational changes observed in enzyme crystal structures upon substrate binding. *J. Mol. Biol. 346*, 21–28.
45. MacRae, I. J., Li, F., Zhou, K., Cande, W. Z., and Doudna, J. A. (2006) Structure of Dicer and Mechanistic Implications for RNAi. *Cold Spring Harbor Symp. Quant. Biol. 71*, 73–80.
46. Ramesh, A., Savva, C. G., Holzenburg, A., and Sacchettini, J. C. (2007) Crystal Structure of Rsr, an Ortholog of the Antigenic Ro Protein, Links Conformational Flexibility to RNA Binding Activity. *J. Biol. Chem. 282*, 14960–14967.
47. Bayer, T. S., Booth, L. N., Knudsen, S. M., and Ellington, A. D. (2005) Arginine-rich motifs present multiple interfaces for specific binding by RNA. *RNA 11*, 1848–1857.
48. Koukiekolo, R., Sagan, S. M., and Pezacki, J. P. (2007) Effects of pH and salt concentration on the siRNA binding activity of the RNA silencing suppressor protein p 19. *FEBS Lett. 581*, 3051–3056.
49. Sullivan, C. S., Grundhoff, A. T., Tevethia, S., Pipas, J. M., and Ganem, D. (2005) SV40-encoded microRNAs regulate viral gene expression and reduce susceptibility to cytotoxic T cells. *Nature 435*, 682–686.
50. Gupta, A., Gartner, J. J., Sethupathy, P., Hatzigeorgiou, A. G., and Fraser, N. W. (2006) Anti-apoptotic function of a microRNA encoded by the HSV-1 latency-associated transcript. *Nature 442*, 82–85.

BI800401Y